Biochemical and Biophysical Research Communications 428 (2012) 259–263

Contents lists available at SciVerse ScienceDirect

Biochemical and Biophysical Research Communications

journal homepage: www.elsevier.com/locate/ybbrc

ER-activating ability of breast cancer stromal fibroblasts is regulated independently of alteration of *TP53* and *PTEN* tumor suppressor genes

Tetsuji Suda [a], Hanako Oba [b], Hiroyuki Takei [c], Masafumi Kurosumi [b], Shin-ichi Hayashi [d,e], Yuri Yamaguchi [a,*]

[a] *Research Institute for Clinical Oncology, Saitama Cancer Center, Ina-machi, Saitama 362-0806, Japan*
[b] *Department of Pathology, Saitama Cancer Center, Ina-machi, Saitama 362-0806, Japan*
[c] *Division of Breast Surgery, Saitama Cancer Center, Ina-machi, Saitama 362-0806, Japan*
[d] *Department of Molecular and Functional Dynamics, Graduate School of Medicine, Tohoku University, Aoba-ku, Sendai 980-8575, Japan*
[e] *Center for Regulatory Epigenome and Diseases, Graduate School of Medicine, Tohoku University, Aoba-ku, Sendai 980-8575, Japan*

ARTICLE INFO

Article history:
Received 2 October 2012
Available online 12 October 2012

Keywords:
Carcinoma-associated fibroblasts (CAF)
Estrogen
Estrogen receptor (ER)
Breast cancer

ABSTRACT

Carcinoma-associated fibroblasts (CAFs) are associated with tumor progression and metastasis, and are able to activate estrogen receptor (ER) in breast cancer. We established a stable transformant of a human breast cancer cell line to detect CAF-specific ER-activating ability, and found that this CAF ability varied among tumors. Some studies have reported a high frequency of alterations among tumor suppressor genes in stromal cells, but do not generally agree as to the frequency. Moreover, the activation mechanism of CAF-induced estrogen signals, including the effects of these gene aberrations, is not fully understood. We investigated the relevance of tumor suppressor gene aberrations and ER-activating ability in CAFs derived from 20 breast cancer patients. Although CAF-specific ER-activating abilities varied among individual cases, all CAFs maintained wild-type alleles for *TP53* and *PTEN*. Also, copy number aberrations in these genes were not observed in any CAFs. Our results suggest that the ER-activating ability of the CAFs is regulated independently of aberrations in these genes; and that other mechanisms of tumor–stromal interaction may affect activation of estrogen signals in breast cancer.

1. Introduction

Carcinoma-associated fibroblasts (CAFs) in proximity to epithelial tumor cells have been associated with tumor-promoting roles in various human carcinomas. In the human prostate cancer model, CAFs have been grown with initiated nontumorigenic epithelial cells, stimulated tumor growth and altered histology of epithelial cells [1]. Significant evidence also shows that CAFs regulate tumor angiogenesis in neuroblastoma and prostate cancer [2,3]. Secreted factors, cytokines and cell surface proteins of CAFs are also associated with metastasis in colon and other tumors [4–6]. However, the activation mechanism of CAFs during tumor development is not yet fully understood.

In breast cancer, CAFs are similarly associated with tumor growth, metastasis and poor clinical outcome, and enhance tumor angiogenesis in comingled breast cancer cells [7,8]. Over two thirds of breast cancers express estrogen receptors (ERs), which can be mediated by two distinct types of signaling, often referred to as the genomic pathway, and the non-genomic or non-genotropic pathways. Therefore ERα expression is predictive of response to endocrine therapy to reduce estrogen stimulation for proliferation. While selective ER modulators (SERMs), including tamoxifen, have been used as first-line hormonal therapy for postmenopausal patients for many years, aromatase inhibitors (AIs) including letrozole, anastrozole and exemestane have shown benefit by minimizing risk of early relapse in advanced disease; AIs are potent inhibitors of aromatase activity that locally converts androgens into estrogens in a variety of tissues including muscle, connective tissue, skin and liver [9,10]. The CAFs in the vicinity of breast cancer tissues are known to express aromatase [11,12], and are target of AIs, which have now largely replaced tamoxifen as first-line therapy in the postmenopausal breast cancer [13,14].

High mutation frequencies for *TP53* and/or *PTEN* were described in CAFs of breast cancer tissue [15,16]. In addition, loss of heterozygosity (LOH) in *TP53*, *PTEN* and other loci was reported in CAFs [15–17]; such mutations and CAF-specific LOH were associated with lymph node metastasis in sporadic breast cancer [16]. For an *in vivo* model of prostate cancer, Hill et al. found that the selective mutation of *p53* in reactive stroma accelerates spontaneous tumor progression [18]. Although these results suggest that

* Corresponding author. Address: Research Institute for Clinical Oncology, Saitama Cancer Center, 818 Komuro, Ina-machi, Saitama 362-0806, Japan. Fax: +81 48 722 1129.
E-mail address: yamaguchi@cancer-c.pref.saitama.jp (Y. Yamaguchi).

0006-291X/$ - see front matter © 2012 Elsevier Inc. All rights reserved.
http://dx.doi.org/10.1016/j.bbrc.2012.10.035

stromal mutations affect tumor growth and progression, further research has revealed that such mutations are rare events in stromal fibroblasts; this question is still controversial [19–21].

Previously, we reported establishing a stable transformant of a human breast cancer cell line to detect CAF-specific ER-activating ability in the co-culture by transfection with the estrogen-responsive element–GFP. This system is a useful tool for analyzing local ER-related signals and tumor–stromal interactions [22] (Fig. 1). We reported that the ability of CAFs to activate ERs and sensitivity to AIs varied among tumors, and that the analysis of CAF characteristics in an individual breast cancer is essential to prediction of hormone therapy efficacy [22]. However, the mechanism underlying regulation of ER-activating ability in CAFs, including the effects of genomic instability, remains unknown. In this study, we focused on aberrations of the tumor suppressor genes *TP53* and *PTEN* in CAFs of breast cancer, and clarified their relevance to clinicopathological features and ER-activating ability in CAFs.

2. Materials and methods

2.1. Cells and culture conditions

The human breast cancer cell line ERE–GFP-E10, a MCF7 clone stably transfected with the d2E-green fluorescent protein (GFP) vector carrying the ptk-estrogen-responsive element (ERE) insert, was isolated and described previously [22]. ERE–GFP-E10 was maintained in RPMI-1640 medium (Sigma–Aldrich Co., St. Louis, MO) supplemented with 10% fetal bovine serum (FBS).

Human breast cancer tissues were obtained by surgery at the Saitama Cancer Center Hospital (Saitama, Japan) after informed consent was obtained from the patients. The Saitama Cancer Center Ethics Committee approved this study. We have previously described the isolation procedure of intratumoral stromal cells and the characterization of CAFs obtained from individual breast cancer patients [22]. Isolated primary CAFs were maintained in modified minimum essential medium (MEM)-Alpha (Invitrogen, Carlsbad, CA) with 10% FBS. The ER-activating ability of CAFs was detected with GFP signals of ERE–GFP-E10 co-cultured with CAFs after pre-culture in phenol red-free RPMI 1640 with dextran-coated and charcoal-treated 10% FCS (DCC–FCS); ability to activate ER had been previously evaluated by the individual value of the ratio of GFP-positive cells for CAFs from 20 breast cancers [22].

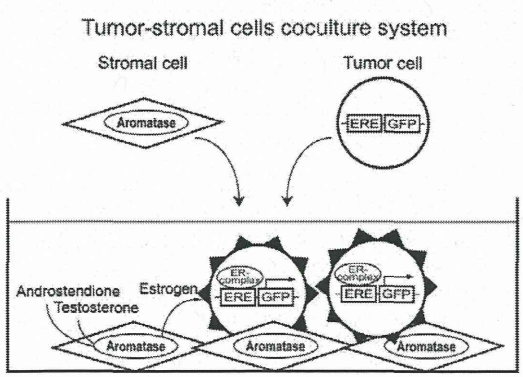

Fig. 1. Many breast cancer stromal fibroblasts can activate estrogen receptors (ER) and accelerate breast cancer proliferation and progression via the ER. Our established system detects ER-activating ability of CAFs by GFP signals of this human breast cancer cell line, and is useful for analysis of the local estrogen signaling pathway. ER: estrogen receptor; ERE: estrogen-responsive element.

2.2. Nucleic acid preparation

For genomic DNA isolation, a QIAamp DNA Mini Kit (Qiagen KK, Tokyo, Japan) was used for CAFs from breast cancers and peripheral blood leukocytes from healthy volunteer, according to the manufacturer's instructions. DNA concentration and purity were determined by Nanodrop® ND-1000 Spectrophotometer (Laboratory & Medical Supplies, Tokyo, Japan), and then stored at −20 °C until analysis.

2.3. PCR amplification

The three fragments of *TP53* (corresponding to exon 4, exons 5–6 and exons 7–8) were amplified from genomic DNA extracted from CAFs for each case by polymerase chain reaction (PCR). The amplification conditions for exons 5–8 of *TP53* have been described in our previous report [23], with minor modifications. The primers for exon 4 were synthesized according to the IARC protocols of *TP53* direct sequencing (http://www-p53.iarc.fr/p53sequencing.html). Primer sequences of all sets are described in Additional file 1. The primers used for exons 1–9 of *PTEN* have been reported previously [24–26] (Additional file 1). PCR amplification was carried out in a total volume of 20 μl, consisting of 50 ng of DNA, 1× PrimeSTAR Buffer (Takara Bio Inc., Shiga, Japan), 200 μM dNTPs, 200 nM of each PCR primer, and 0.5 U of PrimeSTAR® HS DNA Polymerase (Takara Bio Inc.). PCR amplification was performed for 30–35 cycles of denaturation at 98 °C for 10 s, annealing at 55–63 °C for 5 s, and extension at 72 °C for 30 s. Annealing temperatures for each primer were shown in Additional file 1. Real-time RT-PCR was performed using a LightCycler® Carousel-Based System (Roche Diagnostics GmbH Mannheim, Germany) to analyze relative amounts of *CYP19A1* (Aromatae) mRNA; the averaged value of 12 samples in this standard curve method was used as cut-off value. The *CYP19A1* expression status of CAFs, including all 67 in our previous report [22], will be described elsewhere.

2.4. DNA sequence

Mutation analysis of *TP53* and *PTEN* was performed by direct sequencing. The purified PCR products were directly sequenced with upstream or downstream primers (Additional file 1) using Big Dye® Terminators v1.1 Cycle Sequencing Kit and ABI PRISM® 310 Genetic Analyzer (Life Technologies Corporation, Rockville, MD). The obtained nucleotide sequences were compared with the reference sequence of *TP53* and *PTEN* (GenBank accession number X54156 and AF067844, respectively).

2.5. Copy number analysis

TaqMan® Copy Number Assays (Life Technologies Corporation) were used to analyze loss of heterozygosity (LOH) of *TP53* and *PTEN* genes. PCR was performed using an Applied Biosystems 7300 Real-time PCR system (Life Technologies Corporation), and TaqMan® Copy Number Assays for *TP53* (Hs05516623_cn) and *PTEN* (Hs05177393_cn) were purchased from Life Technologies Corporation. PCR was performed with TaqMan® Genotyping Master Mix (Life Technologies Corporation) according to the manufacturer's instructions. PCR amplification was carried out in a total volume of 10 μl; the reaction mixture comprised 10 ng of DNA, 1× TaqMan® Copy Number Assay and 1× TaqMan® Copy Number Reference Assay RNase P. PCR amplification was performed using following conditions: 50 °C for 2 min, 95 °C for 10 min; and then 45 cycles of 95 °C for 15 s and 60 °C for 1 min. All PCR was performed in duplicate for each sample. Data analysis was carried out using the software CopyCaller v1.0 (Life Technologies

Table 1
Estrogen receptor (ER)-activating ability of CAFs and clinicopathological features of breast cancer patients ($n = 20$).

		ER-activating ability	
		<10% ($n = 7$)	⩾10% ($n = 13$)
ER, *n*	Positive	3	10
	Negative	4	3
PgR, *n*	Positive	1	4
	Negative	6	9
Histology, *n*	Papillotubular Ca.	0	2
	Solid-tubular Ca.	4	5
	Scirrhous Ca.	1	5
	Special types	1	1
	Invasive micropapillary Ca.	1	0
Tumor size, *n*	T1	4	9
	T2	2	4
	T3	1	0
Lymph node metastasis, *n*	N0	3	4
	N1	4	7
	N2	0	1
	Unknown	0	1
Menopausal status, *n*	Premenopausal	2	7
	Postmenopausal	5	6
Aromatase mRNA. *n*	High expression	3	2
	Low expression	3	4
	Unknown	1	7

ER and PgR status was determined using the Allred scoring system or enzyme immunoassay (EIA).
Tumor Allred scores ⩾3, or EIA ⩾15 fmol/mg were considered to be positive specimens in this study.

Corporation). Peripheral blood leukocyte DNA from a healthy volunteer was used to calibrate each experiment.

3. Results

3.1. Patient population and ER-activating ability of CAFs

The ER-activating ability of CAFs and clinicopathological features of the patients included in the study are listed in Tables 1 and 2. ER-activating ability of CAFs was evaluated by co-culture system with ERE–GFP-E10 cells in the presence of testosterone, an aromatase substrate. The ratio of GFP^+ cells was evaluated. Among the 20 breast cancer patients, 7 (35%) showed low ER-activating ability of CAFs (GFP^+ E10 cells <10%) and 13 (65%) were high ER-activating ability of CAFs (GFP^+ E10 cells ⩾10%). Levels similar to estrogen-induced ER-activation were detected in 3 out of 13 high ER-activating patients.

3.2. TP53 and PTEN sequence analysis of CAFs

Many CAFs activate ER in tumor cells by genomic or non-genomic pathways through the estrogen or growth factors, which are produced by the CAF itself. Because CAFs are reportedly associated with high frequency of genetic aberration, CAF-specific ER-activating ability may be affected by genomic instability. To clarify whether the aberrant tumor suppressor genes in CAFs affect the ER-activation, we performed the mutation analysis of *TP53* and *PTEN* gene. The CAF-derived DNA was analyzed for *TP53* mutations in exons 4–8 that corresponded to the sequence-specific DNA-binding domain, and for *PTEN* mutations in exons 1 and 3–9. As in the previous report [25], we could not detect exon 2 of *PTEN*, despite using two different primer sets. As shown in Table 2,

Table 2
Mutation analysis of *TP53* and *PTEN* in CAFs.

CAF No.	GFP positive rate (%)	*TP53*	*PTEN*
1	4.6	wt	wt
2	27.3	wt	wt
3	27.5	wt	wt
4	2.8	wt	wt
5	9.3	wt	wt
6	1.0	wt	wt
7	40.5	wt	wt
8	38.8	wt	wt
9	31.0	wt	wt
10	38.2	wt	wt
11	5.0	wt	wt
12	28.5	wt	wt
13	9.3	wt	wt
14	13.1	wt	wt
15	28.5	wt	wt
16	14.5	wt	wt
17	23.7	wt	wt
18	12.5	wt	wt
19	9.3	wt	wt
20	16.2	wt	wt

wt, wild-type.

mutations were not found among the regions of these genes in all 20 CAF samples. We also examined the genotypes of ten SNP sites to evaluate LOH using this sequence analysis. Seven out of 10 SNP sites (rs55950612, rs56196266, rs1642786, rs1642787, rs1642788, rs1794288, rs35979531) showed homozygous genotypes in all 20 CAF cells (data not shown), and 3 SNP sites showed a heterozygous genotype in at least one sample (Table 3). These results have shown that LOH had not occurred at least in 12 CAF samples for *TP53* and in 1 sample for *PTEN*.

3.3. Copy number analysis of TP53 and PTEN

The copy number of the *TP53* and *PTEN* gene was evaluated by quantitative real-time PCR-based Copy Number Assays for determining LOH. Copy number of *TP53* ranged from 1.73 to 2.39 copies; copy number aberrations were not observed in any CAFs (Fig. 2A). Although the calculated copy number of *PTEN* had extended more widely than that of *TP53*, LOH at these loci was not detected in any CAFs (Fig. 2B; range: 1.62–3.41). Four cases out of the 20 CAFs examined were predicted to show three copies of *PTEN*, with copy numbers of 2.84, 2.85, 3.05 and 3.41 (Fig. 2B). In these cases, no clear correlation was found between the ER-activating ability and *PTEN* gene copy number in CAFs. These results were true of both premenopausal and postmenopausal patients (Fig. 2). In addition, correlation between gene copy number and ER protein expression in tumor specimens were not found (data not shown).

4. Discussion

In the present study, we investigated genomic alterations of *TP53* and *PTEN* genes in breast cancer CAFs, and for the first time, examined their correlation with ER-activating ability of CAFs and clinicopathological features of tumors. Although various ER-activating abilities were detected in individual CAFs, all CAFs tested in this study maintained wild-type alleles for the genes. In addition, in contrast to previous reports [15,16,27], none of these breast-cancer CAFs showed any evidence of LOH in these genes. This genomically stable phenotype in all 20 CAFs agrees with two previous reports that aberration of these genes in CAFs is a rare event [19,21]. Therefore, our results suggest that the ER-activating ability of the CAFs is regulated independently of

Table 3
The genotypes of three SNP sites in CAFs.

CAF No.	*TP53*		*PTEN*
	rs.1042522	rs.12951053	rs.1799734
1	GCG	TTC	TTATC
2	GCG/GGG	TTC	TTATC
3	GCG/GGG	TTC/TGC	TTATC
4	GCG/GGG	TTC/TGC	TTATC
5	GCG/GGG	TTC/TGC	TTATC
6	GCG/GGG	TTC	TTATC/ –
7	GCG	TTC	– / –
8	GCG	TTC	TTATC
9	GCG/GGG	TTC	TTATC
10	GCG/GGG	TTC/TGC	TTATC
11	GGG	TGC	TTATC
12	GCG/GGG	TTC/TGC	TTATC
13	GCG	TTC	TTATC
14	GCG/GGG	TTC/TGC	TTATC
15	GCG	TTC	TTATC
16	GCG/GGG	TTC/TGC	TTATC
17	GCG	TTC	TTATC
18	GCG	TTC	TTATC
19	GCG/GGG	TTC/TGC	TTATC
20	GCG/GGG	TTC/TGC	TTATC

rs, reference SNP clusters number in NCBI's dbSNP database.

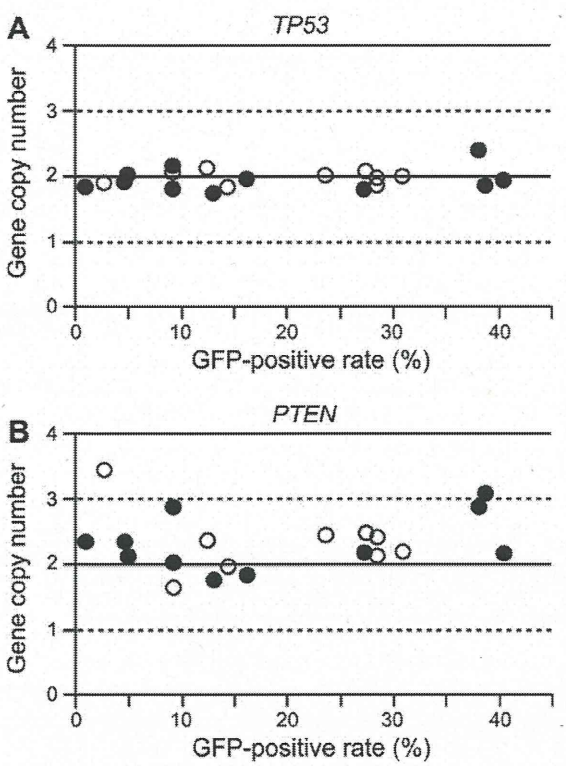

Fig. 2. Copy number analysis and GFP-inducing ability of CAFs. (A and B) Quantitative real-time PCR-based copy number assays for determining loss of heterozygosity (LOH) in CAFs show normal copy number variations of *TP53* (A) and *PTEN* (B). Open and closed circles indicated the menopausal status of premenopausal and postmenopausal patients, respectively.

aberrations in these tumor suppressor genes, and that the mutation or LOH of the genes is rare event.

High frequency mutations and LOH of stromal cells in the previous reports by Kurose et al. and by Patocs et al. have been investigated using DNA derived from microdissected formalin-fixed paraffin-embedded (FFPE) tissues [15,16]. Although obtaining LOH and mutation data from FFPE-derived DNA is a well-established method, low concentrations or low-yield template DNA for PCR might lead to false conclusions [28]. Consequently, the existence of frequent genetic alterations in CAFs is still controversial [19–21]. In this study, we investigated DNA from short-term cultured mammary fibroblasts, which were isolated from carcinoma-associated regions of tumor masses obtained from breast cancer patients. This isolation method can establish adipose stromal fibroblast cells from tumor masses [29], and avoids contamination by tumor cells and other effects.

In the present experiments, we showed that copy numbers were below the cut-off value at 4 copies, which indicates amplification, although the slight increase in copy number of *PTEN* gene was detected in four out of 20 CAFs. No relation was also found between the CAF-specific ER-activating ability and the gene copy number amplification. Somatic mutation and/or deletion of the *PTEN* tumor suppressor gene have been shown to play a crucial role in proliferation and cell survival [30,31]. While the copy number gain of *PTEN* gene in breast cancer does not significantly affect protein levels [32]. Therefore, it can be speculated that the PTEN in our CAFs is not the main regulating factor in activation of ER in tumor cells. However, two previous studies have reported genome-wide copy number analysis of breast CAF samples, and reported 2 CAFs to show genomic alterations in several loci of chromosomes [19,21]. Therefore, the effects of CAFs with low copy amplification of several genes remain to be elucidated.

As for the analysis of CAF-specific ER-activating ability, the detection system of the GFP-based ERE element had been established by our previous report (Fig. 1). We demonstrated that CAFs of postmenopausal patients did not always have high ER-activating ability. Furthermore, it was shown that GFP induction levels did not always correlate with expression of the aromatase gene in CAFs [22]. These results suggest that the ERE–GFP system is not only activated by the estrogen-dependent pathway, but also by estrogen-independent pathways, such as phosphorylation by growth factor-inducing signals. Nevertheless, our results demonstrated that *TP53* or *PTEN* mutation was not the main regulator in either pathway. In this study, we concluded that CAF-specific ER-activating ability is regulated independently from genetic aberrations; however, methylation patterns of several gene regions in tumor stroma have been shown to be distinctly different from normal breast tissue in one report [33]. Furthermore, other epigenetic modifiers of stromal fibroblasts, such as a microRNA that critically affects tumor suppressor function, have also been reported [34,35]. The functional contribution of ER-activation by CAFs in this microenvironment is still unclear; further studies are needed.

Authors' contributions

T.S. carried out the molecular biological studies and drafted the manuscript. H.O. measured aromatase transcripts with RT-PCR. H.O. and M.K. performed pathological analysis. H.T. collected and analyzed clinical data from breast cancer patients. S.H. reviewed all data, and contributed to the preparation of the manuscript. Y.Y. directed the overall project, and participated in the editing of final manuscript. All authors read and approved the final manuscript.

Acknowledgments

This work was supported by the Advanced research for medical products Mining Programme of the National Institute of Biomedical Innovation (NIBIO) in JAPAN, and by Grants-in-Aid for Young Scientists (B) KAKENHI (23791510) of Japan Society for the Promotion of Science (JSPS). The authors thank Ms. Akiyo Yamashita and Ms. Yuko Seino for their technical assistance.

Appendix A. Supplementary data

Supplementary data associated with this article can be found, in the online version, at http://dx.doi.org/10.1016/j.bbrc.2012.10.035.

References

[1] A.F. Olumi, G.D. Grossfeld, S.W. Hayward, P.R. Carroll, T.D. Tlsty, G.R. Cunha, Carcinoma-associated fibroblasts direct tumor progression of initiated human prostatic epithelium, Cancer Res. 59 (1999) 5002–5011.

[2] J.A. Tuxhorn, S.J. McAlhany, T.D. Dang, G.E. Ayala, D.R. Rowley, Stromal cells promote angiogenesis and growth of human prostate tumors in a differential reactive stroma (DRS) xenograft model, Cancer Res. 62 (2002) 3298–3307.

[3] R. Zeine, H.R. Salwen, R. Peddinti, Y. Tian, L. Guerrero, Q. Yang, A. Chlenski, S.L. Cohn, Presence of cancer-associated fibroblasts inversely correlates with Schwannian stroma in neuroblastoma tumors, Mod. Pathol. 22 (2009) 950–958.

[4] M.A. Huber, N. Kraut, J.E. Park, R.D. Schubert, W.J. Rettig, R.U. Peter, P. Garin-Chesa, Fibroblast activation protein: differential expression and serine protease activity in reactive stromal fibroblasts of melanocytic skin tumors, J. Invest. Dermatol. 120 (2003) 182–188.

[5] H. Nakagawa, S. Liyanarachchi, R.V. Davuluri, H. Auer, E.W. Martin Jr., A. de la Chapelle, W.L. Frankel, Role of cancer-associated stromal fibroblasts in metastatic colon cancer to the liver and their expression profiles, Oncogene 23 (2004) 7366–7377.

[6] L.R. Henry, H.O. Lee, J.S. Lee, A. Klein-Szanto, P. Watts, E.A. Ross, W.T. Chen, J.D. Cheng, Clinical implications of fibroblast activation protein in patients with colon cancer, Clin. Cancer Res. 13 (2007) 1736–1741.

[7] C. Yazhou, S. Wenlv, Z. Weidong, W. Licun, Clinicopathological significance of stromal myofibroblasts in invasive ductal carcinoma of the breast, Tumour Biol. 25 (2004) 290–295.

[8] A. Orimo, P.B. Gupta, D.C. Sgroi, F. Arenzana-Seisdedos, T. Delaunay, R. Naeem, V.J. Carey, A.L. Richardson, R.A. Weinberg, Stromal fibroblasts present in invasive human breast carcinomas promote tumor growth and angiogenesis through elevated SDF-1/CXCL12 secretion, Cell 121 (2005) 335–348.

[9] P.K. Siiteri, Review of studies on estrogen biosynthesis in the human, Cancer Res. 42 (1982) 3269s–3273s.

[10] P.E. Lonning, Aromatase inhibitors in breast cancer, Endocr. Relat. Cancer 11 (2004) 179–189.

[11] R.J. Pauley, S.J. Santner, L.R. Tait, R.K. Bright, R.J. Santen, Regulated CYP19 aromatase transcription in breast stromal fibroblasts, J. Clin. Endocrinol. Metab. 85 (2000) 837–846.

[12] Y. Yamaguchi, Microenvironmental regulation of estrogen signals in breast cancer, Breast Cancer 14 (2007) 175–181.

[13] A. Howell, J. Cuzick, M. Baum, A. Buzdar, M. Dowsett, J.F. Forbes, G. Hoctin-Boes, J. Houghton, G.Y. Locker, J.S. Tobias, Results of the ATAC arimidex tamoxifen alone or in combination trial after completion of 5 years' adjuvant treatment for breast cancer, Lancet 365 (2005) 60–62.

[14] L. Gibson, D. Lawrence, C. Dawson, J. Bliss, Aromatase inhibitors for treatment of advanced breast cancer in postmenopausal women, Cochrane Database Syst. Rev. (2009) CD003370.

[15] K. Kurose, K. Gilley, S. Matsumoto, P.H. Watson, X.P. Zhou, C. Eng, Frequent somatic mutations in PTEN and TP53 are mutually exclusive in the stroma of breast carcinomas, Nat. Genet. 32 (2002) 355–357.

[16] A. Patocs, L. Zhang, Y. Xu, F. Weber, T. Caldes, G.L. Mutter, P. Platzer, C. Eng, Breast-cancer stromal cells with TP53 mutations and nodal metastases, N. Engl. J. Med. 357 (2007) 2543–2551.

[17] N. Wernert, C. Locherbach, A. Wellmann, P. Behrens, A. Hugel, Presence of genetic alterations in microdissected stroma of human colon and breast cancers, Anticancer Res. 21 (2001) 2259–2264.

[18] R. Hill, Y. Song, R.D. Cardiff, T. Van Dyke, Selective evolution of stromal mesenchyme with p53 loss in response to epithelial tumorigenesis, Cell 123 (2005) 1001–1011.

[19] W. Qiu, M. Hu, A. Sridhar, K. Opeskin, S. Fox, M. Shipitsin, M. Trivett, E.R. Thompson, M. Ramakrishna, K.L. Gorringe, K. Polyak, I. Haviv, I.G. Campbell, No evidence of clonal somatic genetic alterations in cancer-associated fibroblasts from human breast and ovarian carcinomas, Nat. Genet. 40 (2008) 650–655.

[20] I. Campbell, K. Polyak, I. Haviv, Clonal mutations in the cancer-associated fibroblasts the case against genetic coevolution, Cancer Res. 69 (2009) 6765–6768.

[21] A.N. Hosein, M. Wu, S.L. Arcand, S. Lavallee, J. Hebert, P.N. Tonin, M. Basik, Breast carcinoma-associated fibroblasts rarely contain p53 mutations or chromosomal aberrations, Cancer Res. 70 (2010) 5770–5777.

[22] Y. Yamaguchi, H. Takei, K. Suemasu, Y. Kobayashi, M. Kurosumi, N. Harada, S. Hayashi, Tumor-stromal interaction through the estrogen-signaling pathway in human breast cancer, Cancer Res. 65 (2005) 4653–4662.

[23] T.I. Godai, T. Suda, N. Sugano, K. Tsuchida, M. Shiozawa, H. Sekiguchi, A. Sekiyama, M. Yoshihara, S. Matsukuma, Y. Sakuma, E. Tsuchiya, Y. Kameda, M. Akaike, Y. Miyagi, Identification of colorectal cancer patients with tumors carrying the TP53 mutation on the codon 72 proline allele that benefited most from 5-fluorouracil (5-FU) based postoperative chemotherapy, BMC Cancer 9 (2009) 420.

[24] Y.C. Hu, K.Y. Lam, J.C. Tang, G. Srivastava, Mutational analysis of the PTEN/MMAC1 gene in primary oesophageal squamous cell carcinomas, Mol. Pathol. 52 (1999) 353–356.

[25] X.H. Li, H.C. Zheng, H. Takahashi, S. Masuda, X.H. Yang, Y. Takano, PTEN expression and mutation in colorectal carcinomas, Oncol. Rep. 22 (2009) 757–764.

[26] J. Yang, Y. Ren, L. Wang, B. Li, Y. Chen, W. Zhao, W. Xu, T. Li, F. Dai, PTEN mutation spectrum in breast cancers and breast hyperplasia, J. Cancer Res. Clin. Oncol. 136 (2010) 1303–1311.

[27] K. Kurose, S. Hoshaw-Woodard, A. Adeyinka, S. Lemeshow, P.H. Watson, C. Eng, Genetic model of multi-step breast carcinogenesis involving the epithelium and stroma clues to tumour-microenvironment interactions, Hum. Mol. Genet. 10 (2001) 1907–1913.

[28] S.E. Kern, J.M. Winter, Elegance silence and nonsense in the mutations literature for solid tumors, Cancer Biol. Ther. 5 (2006) 349–359.

[29] R.L. Van, C.E. Bayliss, D.A. Roncari, Cytological and enzymological characterization of adult human adipocyte precursors in culture, J. Clin. Invest. 58 (1976) 699–704.

[30] J. Li, C. Yen, D. Liaw, K. Podsypanina, S. Bose, S.I. Wang, J. Puc, C. Miliaresis, L. Rodgers, R. McCombie, S.H. Bigner, B.C. Giovanella, M. Ittmann, B. Tycko, H. Hibshoosh, M.H. Wigler, R. Parsons, PTEN a putative protein tyrosine phosphatase gene mutated in human brain breast and prostate cancer, Science 275 (1997) 1943–1947.

[31] A. Di Cristofano, B. Pesce, C. Cordon-Cardo, P.P. Pandolfi, Pten is essential for embryonic development and tumour suppression, Nat. Genet. 19 (1998) 348–355.

[32] B. Marty, V. Maire, E. Gravier, G. Rigaill, A. Vincent-Salomon, M. Kappler, I. Lebigot, F. Djelti, A. Tourdes, P. Gestraud, P. Hupe, E. Barillot, F. Cruzalegui, G.C. Tucker, M.H. Stern, J.P. Thiery, J.A. Hickman, T. Dubois, Frequent PTEN genomic alterations and activated phosphatidylinositol 3-kinase pathway in basal-like breast cancer cells, Breast Cancer Res. 10 (2008) R101.

[33] M. Hu, J. Yao, L. Cai, K.E. Bachman, F. van den Brule, V. Velculescu, K. Polyak, Distinct epigenetic changes in the stromal cells of breast cancers, Nat. Genet. 37 (2005) 899–905.

[34] A. Bronisz, J. Godlewski, J.A. Wallace, A.S. Merchant, M.O. Nowicki, H. Mathsyaraja, R. Srinivasan, A.J. Trimboli, C.K. Martin, F. Li, L. Yu, S.A. Fernandez, T. Pecot, T.J. Rosol, S. Cory, M. Hallett, M. Park, M.G. Piper, C.B. Marsh, L.D. Yee, R.E. Jimenez, G. Nuovo, S.E. Lawler, E.A. Chiocca, G. Leone, M.C. Ostrowski, Reprogramming of the tumour microenvironment by stromal PTEN-regulated miR-320, Nat. Cell Biol. 14 (2012) 159–167.

[35] K.K. Wentz-Hunter, J.A. Potashkin, The role of miRNAs as key regulators in the neoplastic microenvironment, Mol. Biol. Int. 2011 (2011) 839872.

Biochemical and Biophysical Research Communications 443 (2014) 1148–1154

Contents lists available at ScienceDirect

Biochemical and Biophysical Research Communications

journal homepage: www.elsevier.com/locate/ybbrc

Centrosomal BRCA2 is a target protein of membrane type-1 matrix metalloproteinase (MT1-MMP)

Nadila Wali [a,d], Kana Hosokawa [a], Sadiya Malik [a], Hiroko Saito [b], Ken Miyaguchi [a], Shinobu Imajoh-Ohmi [c], Yoshio Miki [a,b,*], Akira Nakanishi [a]

[a] Department of Molecular Genetics, Medical Research Institute, Tokyo Medical and Dental University (TMDU), Japan
[b] Department of Molecular Diagnosis, Cancer Institute, The Japanese Foundation of Cancer Research (JFCR), Japan
[c] Medical Proteomics Laboratory, The Institute of Medical Science, The University of Tokyo, Japan
[d] Department of Obstetrics and Gynecology, Urumqi Friendship Hospital, Xinjiang, PR China

ARTICLE INFO

Article history:
Received 6 December 2013
Available online 30 December 2013

Keywords:
BRCA2
MT1-MMP
Centrosome

ABSTRACT

BRCA2 localizes to centrosomes between G1 and prophase and is removed from the centrosomes during mitosis, but the underlying mechanism is not clear. Here we show that BRCA2 is cleaved into two fragments by membrane type-1 matrix metalloproteinase (MT1-MMP), and that knockdown of MT1-MMP prevents the removal of BRCA2 from centrosomes during metaphase. Mass spectrometry mapping revealed that the MT1-MMP cleavage site of human BRCA2 is between Asn-2135 and Leu-2136 (^{2132}LSNN/LNVEGG^{2141}), and the point mutation L2136D abrogated MT1-MMP cleavage. Our data demonstrate that MT1-MMP proteolysis of BRCA2 regulates the abundance of BRCA2 on centrosomes.

1. Introduction

Germline mutations of BRCA2 (breast cancer type 2 susceptibility gene) that truncate the encoded protein result in increased predisposition to cancers of the breast, ovaries [1], and pancreas [2]. Although the role of BRCA2 inactivation in sporadic carcinogenesis remains unclear, several studies have provided evidence that loss of BRCA2 facilitates cancer cell proliferation [3]. BRCA2 is a large protein consisting of 3418 amino acids, including a nuclear localization signal (NLS), centrosomal localization signal (CLS), and nuclear export sequence (NES), and plays multiple roles in repair of DNA double-stand breaks (DSBs), centrosome replication [4], and cytokinesis [5]. In human cell lines, the level of BRCA2 is regulated throughout the cell cycle: expression is low in G0 and G1 phase, but increases as the cell enters S phase [6].

Tight control of cell-cycle progression is ensured by multiple mechanisms, including ubiquitination of G1 cyclin and CDK inhibitors. For example, Skp2 targets numerous substrates such as p27 [7] and BRCA2 for degradation [8]. Previous studies have shown that BRCA2 is localized to the centrosomes during interphase and prophase, but not after prophase [4]. The mechanism by which BRCA2 is removed from the centrosomes during mitosis is not yet clear; to date, ubiquitinated BRCA2 has not been detected at centrosomes. Changes in protein levels over the course of the cell cycle are regulated by ubiquitin-independent proteolysis as well as by the ubiquitin–proteasome system. Several proteolytic activities have been localized to centrosomes, including MT1-MMP, initially described for its role in proteolytic cleavage of the membrane-tethered MMP subfamily [9]. Although best known for its pericellular activities, endocytosed MT1-MMP has also been shown to traffic to the centrosome [10], where it cleaves centrosomal pericentrin. Furthermore, MT1-MMP has been reported to exhibit the preference of cleavage sites [11]. The *MEROPS* database (http://merops.sanger.ac.uk/) includes a collection of known cleavage sites in protease substrates [12,13].

Here, we provide compelling evidence that BRCA2 is cleaved by MT1-MMP. MT1-MMP-depleted cells exhibited elevated levels of wild-type BRCA2 and reduced levels of BRCA2 cleavage. Furthermore, BRCA2 exhibited centrosomal localization during metaphase in MT1-MMP-depleted cells. Finally, expression of wild-type BRCA2 was inversely correlated with the level of BRCA2 cleavage over the course of the cell cycle. Taken together, these results demonstrate that the abundance of BRCA2 protein on centrosomes is controlled by MT1-MMP.

2. Materials and methods

2.1. Plasmid and antibodies

FLAG-tagged BRCA2 protein was generated by fusing sequence encoding the FLAG epitope to the 3′ end of the BRCA2 gene, thereby

* Corresponding author at: Department of Molecular Genetics, Medical Research Institute, Tokyo Medical and Dental University, 1-5-45, Yushima, Bunkyo-ku, Tokyo 113-8510, Japan. Fax: +81 3 5803 5828.
E-mail address: miki.mgen@mri.tmd.ac.jp (Y. Miki).

0006-291X/$ - see front matter © 2013 Elsevier Inc. All rights reserved.
http://dx.doi.org/10.1016/j.bbrc.2013.12.103

creating gene encoding the BRCA2 protein with a carboxy-terminal FLAG tag. GST-tagged BRCA2 (amino acids [a.a.] 1968–2135) protein was generated by fusing sequence encoding GST to the 5′ end of the BRCA2 gene, thereby creating a gene encoding the BRCA2 protein with an N-terminal GST tag. HA-tagged BRCA2 (a.a. 1596–2280) protein was generated by fusing sequence encoding the HA epitope 5′ to BRCA2 gene, thereby creating gene encoding the BRCA2 protein with an N-terminal HA tag. The following commercially available antibodies were used in this study: anti-BRCA2 rabbit polyclonal antibody (pAb) (Ab123491, Abcam, Cambridge, UK); anti-BRCA2 mouse monoclonal antibody (mAb) (Ab-1, Calbiochem); anti-BRCA2 rabbit pAb (H-300 and H-299, Santa Cruz Biotechnology, Dallas, TX, USA); anti-HA rat mAb (3F10, Cell Signaling Technology, Danvers, MA, USA); anti-FLAG mAb (F3165, Sigma–Aldrich, St. Louis, MO, USA); anti-BRCA2 rabbit pAb (5.23, Merck Millipore, Billerica, MA, USA); anti-MT1-MMP [LEM-2/63.1] catalytic domain mouse mAb (ab78738, Abcam); anti-β-actin mAb (AC-74, Sigma–Aldrich); anti-PCNA mAb (5A10, MBL, Nagoya, Japan).

2.2. Peptide synthesis and antibody preparation

Peptides were synthesized by the solid-phase method on an Applied Biosystems Model 430A peptide synthesizer, and purified by reverse-phase high performance liquid chromatography on a C18 column. The following antibodies were generated in rabbits, using synthetic peptides as haptens conjugated to keyhole limpet hemocyanin (KLH), and purified from antisera by affinity chromatography using immobilized antigen peptides: brca2n, which recognizes the N-terminal cleavage fragment of BRCA2, raised against residues 2126–2135 (CSKEFKLSNN); and brca2c, which recognizes the C-terminal cleavage fragment of BRCA2, raised against residues 2136–2149 (LNVEGGSSENNHSI). Antibody titer in antiserum was monitored by dot-blot assay. When the antibody titer increased sufficiently, rabbits were bled from the ear artery (30–50 ml).

2.3. Cell culture and transfection

HeLa S3 cells were purchased from the RIKEN GenBank (Ibaraki, Japan) and cultured in Dulbecco's Modified Eagle Medium (DMEM; Nissui Pharmaceutical, Tokyo, Japan) supplemented with 10% fetal bovine serum (FBS). Other cell lines, U2OS cells, and MCF7 cells were obtained from ATCC (Manassas, VA, USA). HA-BRCA2 and BRCA2-FLAG were expressed into HeLa S3 cells. HeLa S3 cells were synchronized in S phase by a double-thymidine block (DTB): cells were incubated in 2.5 mM thymidine for 18 h, washed with PBS, released for 9 h, and then blocked for another 15 h in 2.5 mM thymidine.

2.4. Immunoblotting and immunoprecipitation (IP) analysis

Anti-normal rabbit IgG or anti-BRCA2 antibody was added to the HeLa S3 cells extract and incubated for 30 min at 4 °C with shaking. Protein G-Sepharose (20 μl of 50% suspension) was added, and the mixture was further incubated for 1 h at 4 °C with shaking. Immunoprecipitates were washed five times with cell lysis buffer containing protease inhibitors. After washing, samples were subjected to SDS–PAGE and transferred electrophoretically onto 0.45-μm PVDF membranes (Merck Millipore). The membranes were stained with primary antibodies for 2 h at RT, followed by incubation for 1 h at RT with secondary antibodies coupled to horseradish peroxidase (ECL anti-mouse or -rabbit IgG; Amersham/GE Healthcare, Buckinghamshire, UK). The blots were developed using the SuperSignal enhanced chemiluminescence reagent (Pierce, Rockford, IL, USA) and exposed to Kodak X-OMAT film.

2.5. Mass-spectrometry analysis

The samples immunoprecipitated for full-length BRCA2 were subjected to SDS–PAGE, and the gels were stained with SYPRO Ruby Protein Gel Stain (Molecular Probes/Life Technologies, Carlsbad, CA, USA). The stained gel bands around 250 kDa were cut out and treated with dithiothreitol (DTT, Nacalai Tesque, Kyoto, Japan) dissolved in ammonium hydrogen carbonate (Nacalai Tesque), followed by treatment with iodoacetamide (Wako, Osaka, Japan). After the gels were dried, 20 μl of 0.05 pmol/μl trypsin (AB SCIEX, Framingham, MA, USA) solution was applied to each gel piece and incubated for 14 h at 37 °C to digest proteins. Digested peptides were extracted by washing the gel pieces twice with 50% trifluoroacetic acid (TFA, Wako), followed by washing with 80% TFA. The purified peptide samples were injected onto a reversed-phase C18 column (HiQ sil C18W-3P, 3 μm, 120 Å, KYA TECH Corp.) and separated by nanoflow liquid chromatography (300 nL/min) on a nano LC Dina-A system (KYA TECH Corp.) in line with a Q-TRAP 5500 instrument (AB SCIEX). A synthesized peptide that is recognized by MT-MMP1 (LSNNLNVEGG) and a mutant derivative (LSNNDNVEGG) were subjected to similar analysis following digestion.

2.6. Immunofluorescence (IF) analysis

HeLa S3 cells were fixed for 10 min on ice in 3.7% formaldehyde in PBS, and then sequentially permeabilized by incubation in 50%, 75%, and 95% ethanol solutions on ice for 5 min each. Slides were blocked with PBS containing blocking solution for 30 min at RT, incubated with primary antibody for 1 h at RT, and then washed three times with PBS. Next, cells were incubated with Alexa Fluor 488- or Alexa Fluor 594- conjugated secondary antibody (Molecular Probes; Life Technologies) for 1 h at RT, washed three times with PBS, and preserved in Vectashield (Vector Inc., Burlingame, CA, USA).

2.7. FACS analysis

HeLa cells were arrested at S phase by DTB. At various times, cells were washed with PBS, and then fixed in 70% ethanol solution. Fixed cells were washed twice with PBS, and then treated with RNase A at 37 °C for 30 min. Finally, cells were stained with propidium iodide and incubated in the dark for 30 min. Samples were analyzed by flow cytometry using fluorescence activated cell sorting (FACS, BD Bioscience, San Jose, CA). A total of 10,000 cells were counted for each sample. Gating of cell populations and quantitation were performed using the ModFit LT™ program provided by the Verity Software House.

2.8. MT1-MMP activity assay

MT1-MMP activity buffer was 50 mM Tris–HCl (pH 7.4), 150 mM NaCl, 1 mM $CaCl_2$, and 5 μM $ZnCl_2$. Recombinant MT1-MMP catalytic domain and Brij 35 (final concentration: 0.01%) were added to the activity buffer. Anti-HA or anti-FLAG immunoprecipitates from HeLa S3 cells expressing HA-BRCA2 or BRCA2-FLAG were incubated with 100 ng active MT1-MMP for 3 h at 37 °C, followed by immunoblotting with anti-HA or FLAG antibodies. Recombinant MT1-MMP catalytic domain (475935) and a hydroxamate inhibitor (GM6001, N-[(2R)-2-(hydroxamidocarbonylmethyl)-4-methylpentanoyl]-L-tryptophan methylamide) were purchased from CALBIOCHEM (USA). GM6001 was dissolved at a concentration of 25 mM in DMSO.

2.9. Knockdown of BRCA2 and MT1-MMP

Expression of BRCA2 was knocked down using two different siRNAs, BRCA2-1 (5′-GAAACGGACUUGCUAUUUA-3′) and BRCA2-2 (5′-GAAGAAUGCAGGUUUAAUA-3′). Likewise, MT1-MMP was knocked down using two different siRNAs, MT1-MMP-1 (5′-GGAUGGAC ACGGAGAAUUU-3′) and MT1-MMP-2 (5′-GGUCUCAAAUGGCAAC AUA-3′). Cells at about 40% confluence were transfected with siRNAs using Lipofectamine RNAiMAX reagent (Invitrogen; Life Technologies) in Opti-MEM I (Invitrogen; Life Technologies) and cultured in 5% CO_2 at 37 °C for 72 h.

3. Results

3.1. Detection of cleaved BRCA2 in cancer cells

The positions of the binding sites of BRCA2 antibodies are summarized in Fig. 1A. Using the antibodies Ab123491, Ab-1, and 5.23, full-length BRCA2 (384 kDa) was detected in several cell lines (Fig. 1B; lanes 1–6). Simultaneously, an approximately 250-kDa protein was also detected in cell lines other than MCF-7 using the Ab123491 and Ab-1 antibodies (Fig. 1B; lanes 1–5). By contrast, no 250-kDa protein was detected using the 5.23 antibody (Fig. 1B; lane 6). In order to confirm whether the 250-kDa protein was derived from BRCA2, we made use of specific BRCA2 siRNAs and the Ab123491 antibody. Fig. 1C shows that siRNAs against BRCA2 specifically reduced the level of full-length BRCA2 (384 kDa) and also significantly reduced the level of the 250-kDa protein, as revealed by immunoblotting for BRCA2. To further confirm the identity of the 250-kDa protein, anti-BRCA2 immunoprecipitate was subjected to SDS–PAGE followed by SYPRO RUBY staining, and the 250-kDa region of the gel was cut out and subjected by nano-LC–MS/MS. The mass-spectrometry analysis detected both BRCA2 and MT1-MMP (Fig. 1D). These results suggest the presence of a cleaved fragment of BRCA2 in several cancer cell lines.

3.2. MT1-MMP cleaves BRCA2

Searching the MEROPS peptidase database revealed the presence of four MT1-MMP cleavage sites (LSG402-L403, SHN1333-L1334, SDN1619-L1620 and SNN2135-L2136) in BRCA2 (Fig. 2A). Calculation of the molecular weights of fragments resulting from the predicted cleavage pattern identified two candidates for the 250-kDa protein described in the previous section (Fragment 1: 239-kDa and Fragment 2: 235-kDa). In order to narrow down the location of the MT1-MMP target cleavage site within BRCA2, we constructed a plasmid for expression of an HA-tagged fragment of BRCA2, HA-BRCA2 (a.a. 1596–2280), which includes the cleavage site, SNN^{2135}-L^{2136}. HA-BRCA2 purified on an HA-affinity column was cleaved into two fragments by active MT1-MMP, and one of the fragments was detected at 62 kDa (Fragment 3) using anti-HA antibody (Fig. 2A and B). When GM6001, an MMP inhibitor, was added to the cleavage reaction, the 62-kDa cleavage fragment was not observed (Fig. 2C). Furthermore, we observed a time-dependent increase in the level of Fragment 3, and a corresponding decrease in level of the original HA-BRCA2, following addition of active MT1-MMP (Fig. 2D). Next, we investigated whether full-length BRCA2 is cleaved by MT1-MMP. Full-length

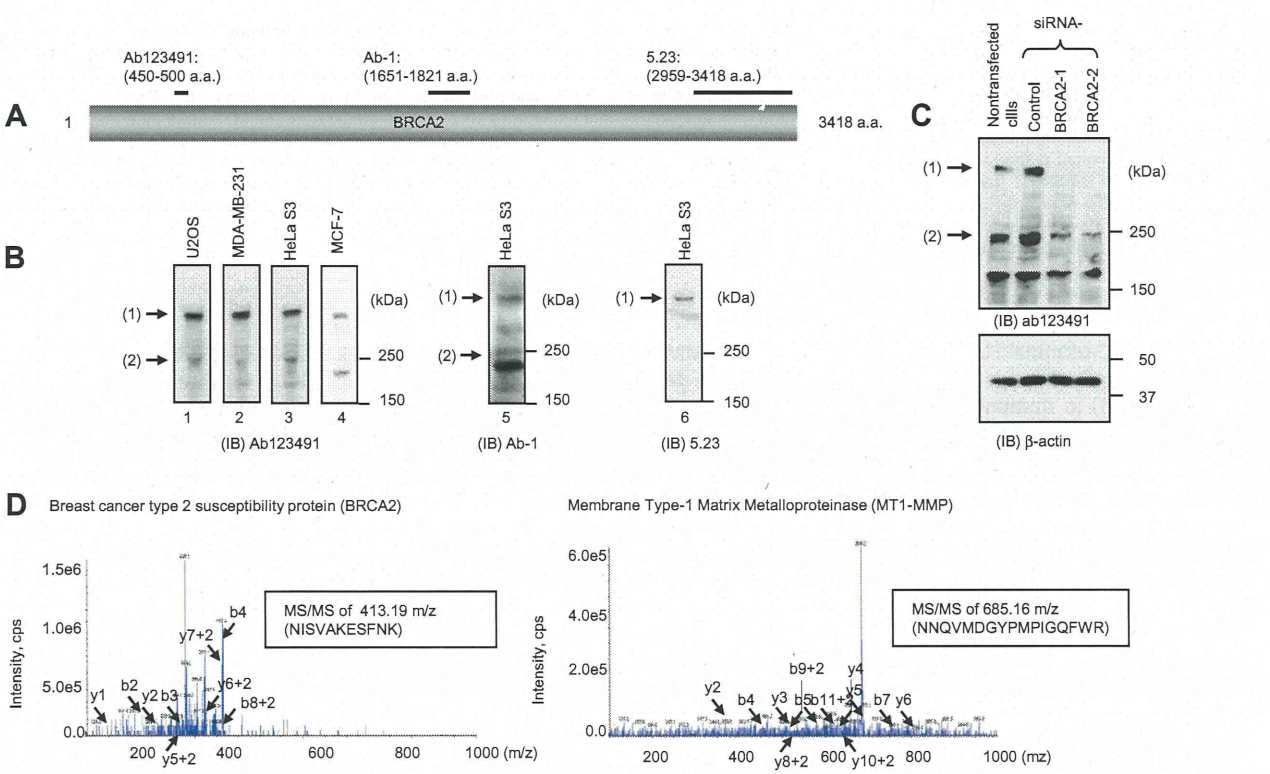

Fig. 1. A BRCA2 fragment of approximately 250 kDa was found in cancer cells and confirmed by mass spectrometry. (A) Schematic of epitope regions for three anti-BRCA2 antibodies. (B) Cell lysates from the indicated cell lines (U2OS, MDA-MB-231, HeLa S3, and MCF-7) were subjected to SDS–PAGE and blotted onto membranes. The blots were probed with antibodies (Ab123491, Ab-1, and 5.23) against BRCA2. Full-length BRCA2 (1) and a BRCA2 fragment of approximately 250 kDa (2) were detected by anti-BRCA2 antibody. (C) HeLa S3 cells were transiently transfected with BRCA2 siRNA (1 or 2), control siRNA, or nontransfected. At 72 h, cells were harvested and subjected to immunoblotting using anti-BRCA2 and anti-β-actin. β-actin was used as a gel loading control. (1) and (2) show full-length BRCA2 and the BRCA2 fragment of approximately 250 kDa, respectively. (D) Anti-BRCA2 and anti-IgG immunoprecipitates were subjected to SDS–PAGE, and the gel was stained with SYPRO RUBY. Gel bands corresponding to approximately 250 kDa were cut out and analyzed by nano-LC MS/MS. Mass spectra for a BRCA2 peptide (a.a. 1435–1445; left panel) and an MT1-MMP peptide (a.a. 346–362; right panel).

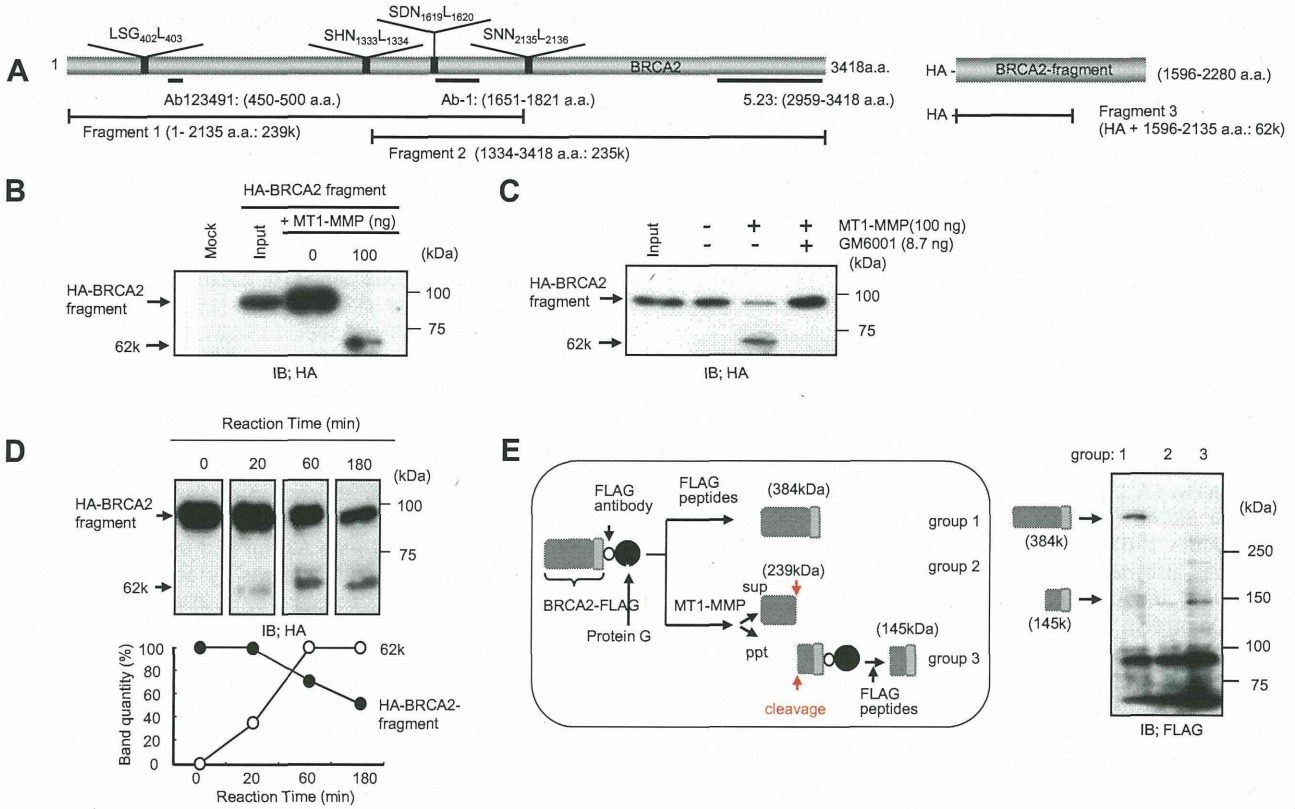

Fig. 2. BRCA2 is cleaved by MT1-MMP *in vitro*. (A) Candidate cleavage sites within BRCA2, and the positions of the BRCA2 antibody binding sites. Based on the positions of putative cleavage sites, we predicted two potential fragments with sizes near 250 kDa (Fragment 1: a.a. 1–2135; Fragment 2: a.a. 1334–3418). We constructed a plasmid vector for expression of the HA-BRCA2 fragment (a.a. 1596–2280 a.a.), and the molecular weight of the predicted MT1-MMP cleavage fragment is shown (Fragment 3: 62-kDa, a.a. 1596–2135). (B) HA-BRCA2 fragment (a.a. 1596–2280) was expressed in HeLa S3 cells and purified using an HA-affinity column. After digestion of purified HA-BRCA2 fragment with active MT1-MMP (100 ng), the reaction products were analyzed by immunoblotting with anti-HA antibody. (C) An MT1-MMP inhibitor, GM6001 (8.7 ng), was added to a reaction mix containing purified HA-BRCA2 fragment and MT1-MMP (100 ng). (D) After incubation of HA-BRCA2 fragment with active MT1-MMP, the digestion products were harvested at several points (0, 20, 60, and 180 min) and analyzed by immunoblotting with anti-HA antibody. The intensities of 62-kDa cleavage polypeptides (white circles) and HA-BRCA2 fragment (black circles) are indicated under the immunoblot image. (E) BRCA2-FLAG was transfected into HeLa S3 cells and collected by immunoprecipitation with anti-FLAG antibody. Precipitates were either not treated (group 1) or treated MT1-MMP1; from the treated samples, supernatant (group 2) and precipitate (group 3) were collected separately. All groups were subjected to SDS–PAGE and immunoblot with anti-FLAG antibody. Group 1 contains full-length FLAG-tagged BRCA2 (384 kDa); group 2 contains N-cBRCA2 without a FLAG tag (no band detected); and group 3 contains C-cBRCA2 with a FLAG tag (145 kDa).

BRCA2 with a C-terminal FLAG tag was cleaved by MT1-MMP, and the FLAG-tagged cleavage fragment was detected at 145 kDa (Fig. 2E, lane 3) in immunoblotting analysis. The other cleavage fragment, which is predicted to be a 239 kDa fragment lacking a FLAG tag, was not detected (Fig. 2E, lane 2).

To determine the MT1-MMP cleavage site within BRCA2 and to confirm the predictions based on the database search, we synthesized a 10-mer peptide (LSNNLNVEGG) derived from the putative cleavage site of BRCA2, and subjected it to cleavage by recombinant polypeptide corresponding to the catalytic domain of human MT1-MMP (abcam; ab38970). We determined the mass of the cleavage product (LNVEGG: 588.2 *m/z*) and the experimental MS/MS spectra by mass spectrometry (Supplemental Fig. S1). A mutant peptide containing a single amino-acid substitution, LSNN^{2135}-D^{2136}NVEGG (L2136D), was resistant to proteolysis by MT1-MMP (data not shown). These data further confirm that BRCA2, which bears the predicted cleavage site (LSNN2135↓L2136NVEGG), is cleaved by MT1-MMP.

3.3. Quantitative changes in C-cBRCA2 during the cell cycle

Next, we generated antibodies, brca2n and brca2c, that specifically recognize the cleavage fragments of BRCA2, N-cBRCA2 (a.a. 1–2135) and C-cBRCA2 (a.a. 2136–3418), respectively. To investigate in detail the subcellular localization of N-cBRCA2 and C-cBRCA2 during the cell cycle, HeLa S3 cells were immunostained with anti-BRCA2, brca2n, and brca2c antibodies (Fig. 3A). During interphase, full-length BRCA2 was localized to dots in the nucleus and widely distributed in the cytoplasm. In metaphase, BRCA2 was uniformly distributed outside the region containing the chromosomes. By contrast, N-cBRCA2 localized in the cytoplasm in interphase and metaphase, whereas C-cBRCA2 localized in the nucleus during interphase but was not detectable in metaphase (Fig. 3A).

Next, we examined the relationship between the levels of full-length and cleaved BRCA2. Fig. 3B shows a typical experiment in which cell-cycle progression was analyzed by flow cytometry up to 24 h after release from double-thymidine block (DTB). Cells were harvested at various times after release, and extracted proteins were analyzed on immunoblots using anti-BRCA2, brca2c, anti-MT1-MMP, and anti-βactin antibodies (Fig. 3C). The expression pattern of full-length BRCA2 was tightly regulated: its levels peaked in early S-phase, but decreased significantly by late S phase (Fig. 3D, left). By contrast, C-cBRCA2 was present throughout the cell cycle, with peak levels in late S phase. The level of MT1-MMP remained relatively constant throughout the cell cycle

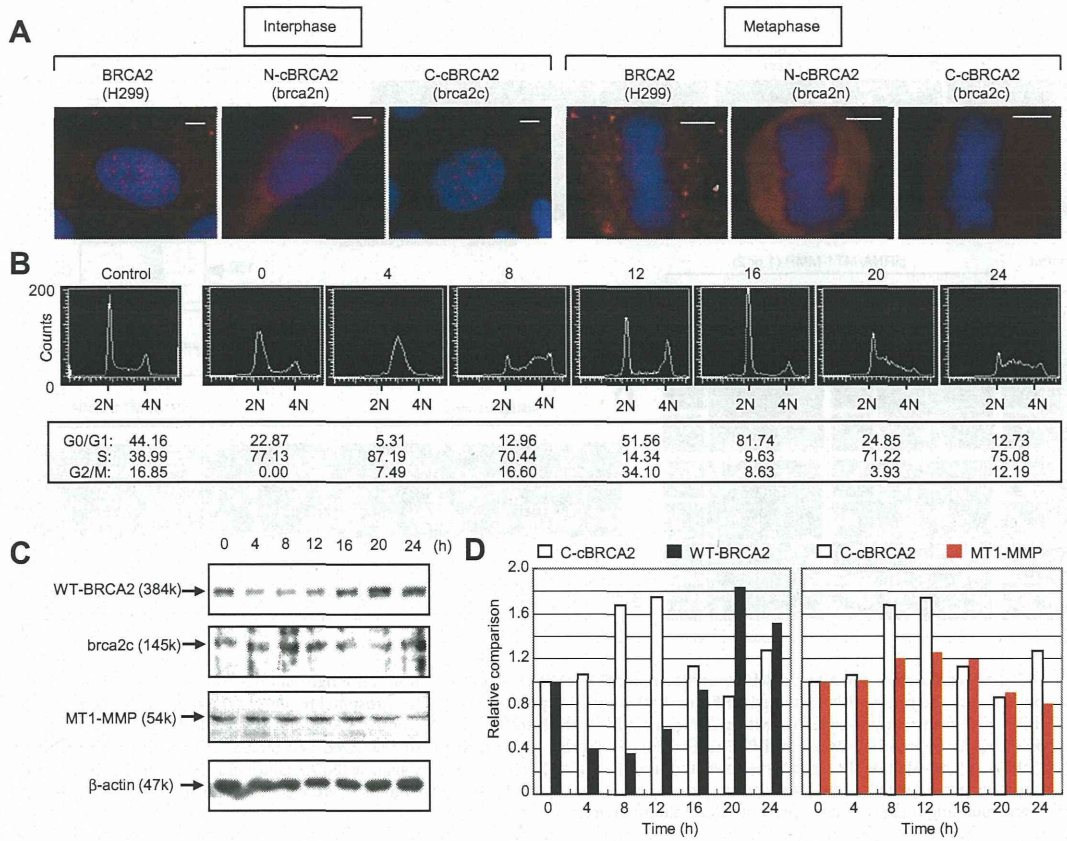

Fig. 3. Quantitative changes in the levels of full-length BRCA2 and C-cBRCA2 over the cell cycle. (A) HeLa S3 cells were fixed and stained for full-length BRCA2 with anti-BRCA2 (H299), for N-cBRCA2 with brca2n, or for C-cBRCA2 with brca2c, followed by staining with Alexa Fluor 594- conjugated anti-rabbit IgG (red). Nuclei are stained with Hoechst (blue). Bar, 5 μm. (B) FACS analysis illustrating the cell-cycle progression of synchronized HeLa S3 cells following release from double-thymidine block. Normal progression through the cell cycle (0 h for early S phase, 4 h for S phase, 8 h for late S to G2 phase, 12 h for G2/M to G0/G1 phase, 16 h for G1 phase, 20 h for late G1 to early S phase, and 24 h for S phase). (C) Total cell lysates were prepared after releasing cells from a double-thymidine-block. Equal quantities of protein from each lysate were subjected to SDS–PAGE followed by immunoblot analysis with anti-BRCA2, brca2c, anti-MT1-MMP, and anti-β-actin antibodies. (D) The column graph at left shows quantitations of full-length BRCA2 (black) and C-cBRCA2 (white) over the course of the cell cycle. The column graph at right shows quantitations of C-cBRCA2 (white) and MT1-MMP (red) over the course of the cell cycle.

(Fig. 3D, right). These results suggest that the levels of cleaved BRCA2 are inversely correlated to those of the full-length protein.

3.4. MT1-MMP cleaves BRCA2 in M phase

The localization of BRCA2 at centrosomes is stringently regulated throughout the cell cycle (Fig. 4A); however the mechanism by which BRCA2 gradually disappears from centrosomes during prophase remains unknown. We observed a marked increase in the level of cleaved BRCA2 during the transition between late S and early M phases (Fig. 3C and D). We hypothesized that the disappearance of BRCA2 from centrosomes could be attributed to cleavage by MT1-MMP. To test this idea, we immunostained cells treated with siRNA against MT1-MMP, or a control siRNA, with anti-BRCA2 and γ-tubulin antibodies, and observed by immunofluorescence microscopy the localization of BRCA2 at centrosomes in metaphase. Immunoblot analysis revealed upregulation of BRCA2 expression in MT1-MMP siRNA-treated cells relative to control siRNA-treated cells (Fig. 4B). Furthermore, as shown in Fig. 4C and D, the BRCA2 signal was stronger at centrosomes in MT1-MMP siRNA-treated cells than in control siRNA-treated cells. Fluorescence intensity profiles along lines drawn between centrosomes revealed the degree of centrosomal staining patterns. These results suggest that the disappearance of BRCA2 from centrosomes during mitosis can be attributed to proteolysis by MT1-MMP.

4. Discussion

The results of this study provide important information regarding BRCA2 proteolysis by MT1-MMP. We demonstrated that a peptide containing the putative cleavage site of BRCA2 (LSNN^{2135}-L^{2136}NVEGG) was cleaved by MT1-MMP (Supplemental Fig. S1), whereas a peptide containing the L2135D substitution was resistant to MT1-MMP. This cleavage site is compatible with the known cleavage preferences of MT1-MMP, and is supported by our biochemical experiments. Furthermore, as shown in Fig. 1B, no 250-kDa fragment of cleaved BRCA2 was detected in MCF-7 cells, which do not express MT1-MMP (Fig. 1B).

MT1-MMP, MMP2, and MMP-9 are associated with tumor invasion and metastasis in ovary [14] and breast carcinomas [15]. Substrates of these MMPs can be divided into four groups according to the selectivity of recognition [16], as follows: (I) substrates recognized by all three MMPs; (II) substrates recognized equally by MT1-MMP and MMP-2; (III) substrates recognized equally by MT1-MMP and MMP-9; and (IV) substrates recognized selectively by MT1-MMP. In this study, we could not determine whether the cleavage site sequence of BRCA2 belongs to any of these groups, because it does not exactly match reported sequences. However, in contrast to the other two MMPs, MT1-MMP is localized to the centrosome, as is the case with BRCA2 [17,10]. In addition, only MT1-MMP was identified in by mass